PHYSICAL REVIEW B **91**, 035430 (2015)

Two-qubit pulse gate for the three-electron double quantum dot qubit

Sebastian Mehl*
Peter Grünberg Institute (PGI-2), Forschungszentrum Jülich, D-52425 Jülich, Germany
and JARA–Institute for Quantum Information, RWTH Aachen University, D-52056 Aachen, Germany
(Received 2 December 2014; revised manuscript received 2 January 2015; published 21 January 2015)

The three-electron configuration of gate-defined double quantum dots encodes a promising qubit for quantum information processing. I propose a two-qubit entangling gate using a pulse-gated manipulation procedure. The requirements for high-fidelity entangling operations are equivalent to the requirements for the pulse-gated single-qubit manipulations that have been successfully realized for Si QDs. This two-qubit gate completes the universal set of all-pulse-gated operations for the three-electron double-dot qubit and paves the way for a scalable setup to achieve quantum computation.

DOI: 10.1103/PhysRevB.91.035430 PACS number(s): 03.67.Lx, 03.65.Yz, 73.21.La, 85.35.Be

I. INTRODUCTION

The name hybrid qubit (HQ) was coined for the qubit encoded in a three-electron configuration on a gate-defined double quantum dot (DQD) [1,2]. The HQ is a spin qubit in its idle configuration, but it is a charge qubit during the manipulation procedure. Recently, impressive progress was made for the single-qubit control of a HQ in Si [3,4]. It was argued that single-qubit gates were implemented, whose fidelities exceed 85% for X rotations and 94% for Z rotations [4]. These manipulations rely on the transfer of one electron between quantum dots (QDs) [2–4]. Subnanosecond gate pulses were successfully applied to transfer the third electron between singly occupied QDs.

Reference [1] suggested two-qubit gates between HQs with similar methods to those for three-electron spin qubits that are defined at three QDs [5,6]. The coupling strength between neighboring QDs is tuned in a multistep sequence, while this entangling gate for HQs requires control over the spin-dependent tunnel couplings. A more realistic approach to realize two-qubit entangling gates for HQs uses electrostatic couplings between the HQs [2]. If the charge configuration of one HQ is changed, then Coulomb interactions modify the electric field at the position of the other HQ. Note the equivalent construction for a controlled phase gate (CPHASE) for singlet-triplet qubits in two-electron DQDs [7].

Using Coulomb interactions for entangling operations can be critical. Even though electrostatic couplings are long-ranged, they are generally weak and they are strongly disturbed by charge noise [8]. I propose an alternative two-qubit gate. Two HQs in close proximity enable the transfer of electrons. The two-qubit gate that is constructed works similarly to the pulse-gated single-qubit manipulations. It requires fast control of the charge configurations on the four QDs through subnanosecond pulse times at gates close to the QDs. A two-qubit manipulation scheme of the same principle as for the single-qubit gates is highly promising because single-qubit pulse gates have been implemented with great success [3,4].

The central requirement of the entangling operation is the tuning of one two-qubit state to a degeneracy point with one leakage state (called $|E\rangle$). The qubit states are $|1\rangle$ and $|0\rangle$, while the subscripts L and R describe the physical positions of the HQs. Specifically, when the state $|0_L0_R\rangle$ is degenerate with $|E\rangle$ then $|0_L0_R\rangle$ can pick up a nontrivial phase, while all the other two-qubit states evolve trivially. Note that a similar construction for an entangling operation [9] has been implemented with impressive fidelities [10–12] for superconducting qubits. The couplings to other leakage states must be avoided during the operation. I propose a two-step procedure. First, $|1_L1_R\rangle$ and $|0_L1_R\rangle$ are tuned away from the initial charge configuration to protect these states from leakage. $|1_L0_R\rangle$ and $|0_L0_R\rangle$ remain unchanged at the same time. One has then reached the readout regime of the second HQ. The second part of the tuning procedure corrects the passage of $|1_L0_R\rangle$ through the anticrossing with $|E\rangle$, at a point where $|1_L0_R\rangle$ is degenerate with another leakage state (called $|L\rangle$). I call this anticrossing degenerate Landau-Zener crossing (DLZC) because the passage through this anticrossing is described by a generalization of the Landau-Zener model [13,14].

I focus on pulse-gated entangling operations for HQs in gate-defined Si QDs. Even though the entangling operation is not specifically related to the material and the qubit design, gate-defined Si QDs are the first candidate where the two-qubit pulse gate might be implemented because Si QDs were used for single-qubit pulse gates [3,4]. I discuss therefore specifically the noise sources that are dominant for experiments involving gate-defined Si QDs. The described two-qubit pulse gates can be directly implemented with the existing methods of the single-qubit pulse gates. It will turn out that high-fidelity two-qubit entangling operations require low charge noise.

The organization of this paper is as follows. Section II introduces the model to describe a pair of three-electron DQDs. Section III constructs the two-qubit gate. Section IV discusses the noise properties of the entangling operation, and Sec. V summarizes all the results.

II. SETUP

I consider an array of four QDs, which are labeled by QD_1–QD_4 (see Fig. 1). One qubit is encoded using a three-electron configuration on two QDs. QD_1 and QD_2 encode HQ_L, and QD_3 and QD_4 encode HQ_R. The system is described by a Hubbard model, which includes two orbital states at each QD. The transfer of electrons between neighboring QDs is possible but weak, unless the system is biased using electric

*s.mehl@fz-juelich.de

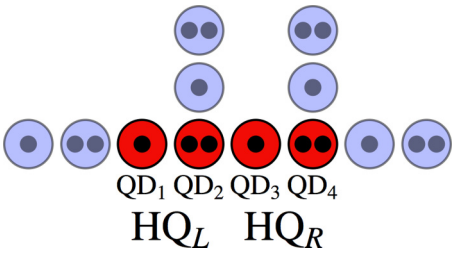

FIG. 1. (Color online) Array of QDs that is used to define and couple HQs. The four red QDs encode two HQs, and they are labeled by HQ_L and HQ_R. Black dots represent electrons. The charge configurations are labeled by the electron numbers $(n_{QD_1},n_{QD_2},n_{QD_3},n_{QD_4})$. (1,2,1,2) is the idle configuration. Applying voltages to gates close to the QDs provides universal single-qubit control and realizes a CPHASE gate by the transfer of single electrons between the QDs. The gate protocols to achieve quantum computation are described in the text. The encoding scheme can be scaled up trivially, as shown by the blue QDs.

gates. It might be desirable to apply a large global magnetic field, which separates states of different s_z energetically. Generally, such a global magnetic field is not needed for the pulse-gated entangling operation because the electron transfer between QDs is spin conserving for weak spin-orbit interactions (as for all Si heterostructures). Also nuclear spin noise only introduces a very small spin-flip probability [15]. Nevertheless, a global magnetic field still reduces the influence of the remaining nuclear spin noise.

The $S=\frac{1}{2}$, $s_z=\frac{1}{2}$ spin subspace of three electrons is two dimensional, and it encodes a qubit [5]. The single-qubit states for HQ_L are $|1_L\rangle=\sqrt{\frac{2}{3}}|{\downarrow}T_+\rangle-\sqrt{\frac{1}{3}}|{\uparrow}T_0\rangle$ and $|0_L\rangle=|{\uparrow}S\rangle$. The first entry in the state notation labels electrons at QD_1, and the second entry labels electrons at QD_2. QD_1 is singly occupied, but two electrons are paired at QD_2. $|S\rangle=c^\dagger_{i\uparrow}c^\dagger_{i\downarrow}|0\rangle$ is the two-electron singlet state at QD_i, $|T_+\rangle=c^\dagger_{i\uparrow}c^\dagger_{\bar{i}\uparrow}|0\rangle$, $|T_0\rangle=\frac{1}{\sqrt{2}}(c^\dagger_{i\uparrow}c^\dagger_{\bar{i}\downarrow}+c^\dagger_{i\downarrow}c^\dagger_{\bar{i}\uparrow})|0\rangle$, and $|T_-\rangle=c^\dagger_{i\downarrow}c^\dagger_{\bar{i}\downarrow}|0\rangle$ are triplet states at QD_i. $c^{(\dagger)}_{i\sigma}$ is the (creation) annihilation operator of one electron in state $|i\rangle$ of QD_i with spin σ, $|i\rangle$ and $|\bar{i}\rangle$ are the ground state and the first excited state at QD_i [16], and $|0\rangle$ is the vacuum state. Similar considerations hold for HQ_R, where QD_3 is singly occupied and QD_4 is filled with two electrons. It is assumed that a two-electron triplet at QD_1 or at QD_3 is strongly unfavored compared to a two-electron triplet at QD_2 or at QD_4. These conditions were fulfilled for the HQs in Refs. [3,4].

The energy $E_0=0$ is assigned to $|0_L0_R\rangle$ in (1,2,1,2). $|1_L0_R\rangle$, $|0_L1_R\rangle$, and $|1_L1_R\rangle$ are higher in energy by Ω_L, Ω_R, and $\Omega_L+\Omega_R$. The excited states $|1_L\rangle$ and $|1_R\rangle$ involve a triplet on a doubly occupied QD that is higher in energy than the singlet configurations of $|0_L\rangle$ and $|0_R\rangle$. Single-qubit gates are not the focus of this work, but I briefly review: all single-qubit gates are applicable through evolutions under σ_x^L, σ_z^L, σ_x^R, and σ_z^R. $\sigma_x=|1\rangle\langle0|+|0\rangle\langle1|$ and $\sigma_z=|1\rangle\langle1|-|0\rangle\langle0|$ are the Pauli operators on the corresponding qubit subspace. They are applied by transferring one electron from QD_2 to QD_1 for HQ_L (and QD_4 to QD_3 for HQ_R). Depending on the pulse profile, pure phase evolutions (described by the operators σ_z^L and σ_z^R) or spin flips (described by the operators σ_x^L and σ_x^R) are created [2–4].

III. TWO-QUBIT PULSE GATE

Two-qubit operations are constructed using the transfer of electrons between neighboring QDs. The charge transfer between (1,2,1,2) and (1,2,2,1) is described by $\mathcal{H}_{34}=\tau_1\sum_{\sigma\in\{\uparrow,\downarrow\}}(c^\dagger_{3\sigma}c_{4\sigma}+\text{H.c.})+\tau_2\sum_{\sigma\in\{\uparrow,\downarrow\}}(c^\dagger_{3\sigma}c_{\bar{4}\sigma}+\text{H.c.})$, where τ_1, τ_2 are tunnel couplings between states from neighboring QDs, and H.c. labels the Hermitian conjugate of the preceding term. $\epsilon_{43}=eV_4-eV_3$ describes the transfer of electrons through voltages applied at gates close to QD_3 and QD_4. Lowering the potential at QD_3 compared to QD_4 favors (1,2,2,1) ($\epsilon_{43}>0$), but (1,2,1,2) is favored for the opposite case ($\epsilon_{43}<0$). (1,2,1,2) and (1,2,2,1) have identical energies at $\epsilon_{43}=\Delta_{43}>\Omega_L,\Omega_R$. Similar considerations hold for the manipulation between (1,2,1,2) and (1,1,2,2), which is described by $\epsilon_{23}=eV_2-eV_3$ and $\mathcal{H}_{23}=\tau_3\sum_{\sigma\in\{\uparrow,\downarrow\}}(c^\dagger_{2\sigma}c_{3\sigma}+\text{H.c.})+\tau_4\sum_{\sigma\in\{\uparrow,\downarrow\}}(c^\dagger_{\bar{2}\sigma}c_{3\sigma}+\text{H.c.})$. (1,2,1,2) and (1,1,2,2) have identical energies at $\epsilon_{23}=\Delta_{23}>\Omega_L,\Omega_R$.

Note that electrostatic couplings between the states of different charge configurations are neglected in this discussion. Reference [2] argued that the Coulomb interaction can introduce energy shifts of $\gtrsim 0.1$ μeV, reaching the magnitudes of the orbital energies (typically 0.1–10 μeV). Coulomb interactions modify the state energies of different charge configurations [we consider only (1,2,1,2), (1,2,2,1), and (1,1,2,2)]. These modifications do not influence the operation principle of the entangling gate because only a two-qubit system with a state degeneracy with one leakage state is required. The Coulomb interactions can be introduced by a shift of the positions of the state degeneracies between different charge configurations.

One can construct an entangling operation in a two-step manipulation procedure, which is shown in Fig. 2. In the first step, ϵ_{43} is modified, and the charge configuration is pulsed from (1,2,1,2) towards (1,2,2,1). Only $|1_R\rangle$ is transferred to $|B\rangle=|(S\uparrow)_R\rangle$ because $|1_R\rangle$ is energetically unfavored compared to $|0_R\rangle$, which remains in (1,2). The tuning uses a rapid pulse to $\epsilon_{43}=\Delta_{43}-\Omega_R$. $\mathcal{H}_{34}$ couples $|1_R\rangle$ and $|B\rangle$ by $\sqrt{\frac{3}{2}}\tau_2$. The occupations of $|1_R\rangle$ and $|B\rangle$ swap after the waiting time $t_1=\frac{h}{2\sqrt{6}\tau_2}$. Afterwards, ϵ_{43} is pulsed to $\epsilon_{43}=\epsilon^*_{43}$, which is far away from all the anticrossings. $|B\rangle$ and $|0_R\rangle$ have the energy difference Ω^*_R at $\epsilon_{43}=\epsilon^*_{43}$. Note that $\epsilon_{43}=\epsilon^*_{43}$ is in the readout regime of HQ_R: $|1_R\rangle$ is in (2,1), but $|0_R\rangle$ is in (1,2).

In the second step, gate pulses modify ϵ_{23} at fixed $\epsilon_{43}=\epsilon^*_{43}$. The charge configuration is pulsed towards (1,1,2,2). States in (1,2,2,1) remain unchanged because they need the transfer of two electrons to reach (1,1,2,2). The states

$$|L\rangle=\left[\sqrt{\frac{1}{6}}|{\uparrow}T_0{\uparrow}\rangle-\frac{\sqrt{3}}{2}|{\uparrow}T_+{\downarrow}\rangle+\frac{1}{2\sqrt{3}}|{\downarrow}T_+{\uparrow}\rangle\right]|S\rangle, \quad (1)$$

$$|\beta\rangle=\tfrac{1}{2}[\sqrt{2}|{\uparrow}T_0{\uparrow}\rangle+|{\uparrow}T_+{\downarrow}\rangle+|{\downarrow}T_+{\uparrow}\rangle]|S\rangle, \quad (2)$$

are introduced. $|E\rangle=|{\uparrow}{\uparrow}SS\rangle$ is the ground state in (1,1,2,2) with $s_z=1$. $\mathcal{H}_{23}$ couples $|0_L0_R\rangle$, $|1_L0_R\rangle$, $|L\rangle$, and $|E\rangle$,

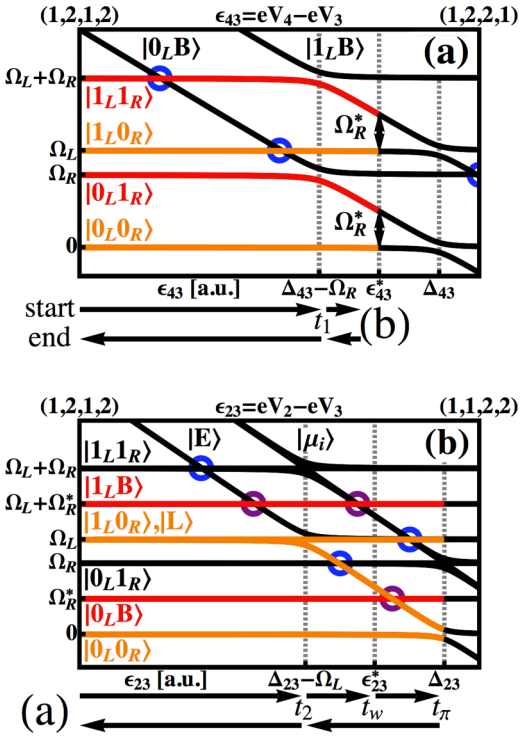

FIG. 2. (Color online) Energy diagram of two coupled HQs with $s_z = 1$ in (1,2,1,2), (1,2,2,1), and (1,1,2,2). The red and the orange lines describe computational basis, and the black lines are leakage states. (1,2,1,2) is favored without external bias. (a) shows the pulsing towards (1,2,2,1), which is modeled through $\epsilon_{43} = eV_4 - eV_3$ describing the potentials at QD_3 and QD_4. The states $|1_L 1_R\rangle$ and $|1_L B\rangle$ as well as $|0_L 1_R\rangle$ and $|0_L B\rangle$ are swapped at $\epsilon_{43} = \Delta_{43} - \Omega_R$. Two of the four state combinations from the computational basis remain in (1,2,1,2) at $\epsilon_{43} = \epsilon^*_{43}$. (b) shows the second step of the manipulation. $\epsilon_{23} = eV_2 - eV_3$ models the potentials at QD_2 and QD_3. As a consequence, only $|1_L 0_R\rangle$ and $|0_L 0_R\rangle$ can be tuned to (1,1,2,2), but $|1_L B\rangle$ and $|0_L B\rangle$ remain in (1,2,2,1). The nontrivial part of the entangling gate is a π-phase evolution of $|0_L 0_R\rangle$ at $\epsilon_{23} = \Delta_{23}$. $|1_L 0_R\rangle$ is degenerate with $|L\rangle$ and passes through a DLZC at $\epsilon_{23} = \Delta_{23} - \Omega_L$. Leakage from the computational subspace is prevented by the pulse cycle that involves waiting times at $\epsilon_{23} = \Delta_{23} - \Omega_L$ and at $\epsilon_{23} = \epsilon^*_{23}$ (see description in the text). The setup is brought back to the initial configuration in the end, by first changing ϵ_{23} and then changing ϵ_{43}. Perfect state crossings are marked, where transitions are forbidden from spin-selection rules (blue), or from charge-selection rules (purple). The waiting times t_1, t_2, t_w, and t_π are given in the text.

while $|\beta\rangle$ is decoupled. When approaching (1,1,2,2), first the anticrossing of $|1_L 0_R\rangle$, $|L\rangle$, and $|E\rangle$ is reached at $\epsilon_{23} = \Delta_{23} - \Omega_L$:

$$\mathcal{H}_{23}(\epsilon_{23}) \approx \begin{pmatrix} \Omega_L & 0 & \frac{\tau_4}{\sqrt{6}} \\ 0 & \Omega_L & -\frac{2\tau_4}{\sqrt{3}} \\ \frac{\tau_4}{\sqrt{6}} & -\frac{2\tau_4}{\sqrt{3}} & \Delta_{23} - \epsilon_{23} \end{pmatrix}. \quad (3)$$

$|0_L 0_R\rangle$ hybridizes with $|E\rangle$ only at $\epsilon_{23} = \Delta_{23}$. $|E\rangle$ has lower energy than $|1_L 0_R\rangle$ at $\epsilon_{23} = \epsilon^*_{23}$, but $|V 0_L 0_R\rangle$ is still the ground state.

The passage through the anticrossing at $\epsilon_{23} = \Delta_{23} - \Omega_L$ is critical for the construction of the entangling operation. $\mathcal{H}_{23}$ describes within the subspace $\{|1_L 0_R\rangle, |L\rangle, |E\rangle\}$ a DLZC [see Eq. (3)]. A basis transformation partially diagonalizes Eq. (3): $|T_1\rangle = \frac{1}{3}|1_L 0_R\rangle - \frac{2\sqrt{2}}{3}|L\rangle$ and $|E\rangle$ have the overlap $\sqrt{3/2}\tau_4$, but $|T_2\rangle = \frac{2\sqrt{2}}{3}|1_L 0_R\rangle + \frac{1}{3}|L\rangle$ is decoupled. $|T_1\rangle$ and $|E\rangle$ swap at $\epsilon_{23} = \Delta_{23} - \Omega_L$ after $t_2 = \frac{h}{2\sqrt{6}\tau_4}$. One introduces the waiting time t_w at $\epsilon_{23} = \epsilon^*_{23}$, where $|E\rangle$ has the energy $\Omega_L/2$. t_w must compensate after the full cycle the relative phase evolution between $|T_1\rangle$ and $|T_2\rangle$; as a consequence, $|1_L 0_R\rangle$ does not leak to $|L\rangle$. Simple mathematics shows that this is the case for $t_w = h(\frac{2n}{\Omega_L} - \frac{1}{\tau_3}) > 0$ with $n \in \mathbb{N}$.

The time evolution at $\epsilon_{23} = \Delta_{23}$ constructs the central part of the entangling gate. $\mathcal{H}_{23}$ couples $|0_L 0_R\rangle$ and $|E\rangle$ by τ_3. The states of the subspace $\{|0_L 0_R\rangle, |E\rangle\}$ pick up a π-phase factor after the waiting time $t_\pi = \frac{h}{2\tau_3}$: $e^{-i\pi\sigma_x} = -\mathbf{1}$. All other states of the computational basis evolve trivially with the energies Ω_L, Ω^*_R, and $\Omega_L + \Omega^*_R$. Finally the setup is tuned back to the initial configuration, involving swaps at $\epsilon_{23} = \Delta_{23} - \Omega_L$ and $\epsilon_{43} = \Delta_{43} - \Omega_R$ that are generated after the waiting times $t_2 = \frac{h}{2\sqrt{6}\tau_4}$ and $t_1 = \frac{h}{2\sqrt{6}\tau_2}$.

In total, the described pulse cycle realizes a CPHASE gate in the basis $|1_L 1_R\rangle$, $|1_L 0_R\rangle$, $|0_L 1_R\rangle$, and $|0_L 0_R\rangle$ when permitting additional single-qubit phase gates:

$$\begin{aligned} &\mathcal{U}_{\epsilon_{43}=\Delta_{43}-\Omega_R}(t_1)\mathcal{U}_{\epsilon_{23}=\Delta_{23}-\Omega_L}(t_2)\mathcal{U}_{\epsilon_{23}=\Delta_{23}}(t_\pi) \\ &\quad \times \mathcal{U}_{\epsilon_{23}=\epsilon^*_{23}}(t_w)\mathcal{U}_{\epsilon_{23}=\Delta_{23}-\Omega_L}(t_2)\mathcal{U}_{\epsilon_{43}=\Delta_{43}-\Omega_R}(t_1) \\ &= e^{\frac{i\pi(p_1+p_2)}{2}} Z_L^{-\frac{p_1}{4}} Z_R^{-\frac{p_2}{4}} \text{CPHASE}, \end{aligned} \quad (4)$$

with $Z_i^\phi = e^{-i2\pi\sigma_z^i\phi}$, $p_1 = \Omega^*_R(\frac{1}{\tau_3} - \frac{2\sqrt{2/3}}{\tau_4} - \frac{4n}{\Omega_L})$, and $p_2 = \Omega_L(\frac{1}{\tau_3} - \frac{2\sqrt{2/3}}{\tau_4})$. $\mathcal{U}_\epsilon(t)$ describes the time evolution at ϵ for the waiting time t. One has constructed a phase shift on HQ_R conditioned on the state of HQ_L. Table I summarizes the manipulation steps of the CPHASE gate.

IV. GATE PERFORMANCE AND NOISE PROPERTIES

In general, two-qubit pulse gates are fast. The only time-consuming parts of the entangling gate are the waiting times at $\epsilon_{43} = \Delta_{43} - \Omega_R$, $\epsilon_{23} = \Delta_{23} - \Omega_L$, $\epsilon_{23} = \epsilon^*_{23}$, and $\epsilon_{23} = \Delta_{23}$. The overall gate time is on the order of $O(\frac{h}{\tau_2}, \frac{h}{\tau_3}, \frac{h}{\tau_4})$. It was shown that tunnel couplings between QDs of a DQD in Si reach 3 μeV [17,18]. Two DQDs might be some distance apart from each other; nevertheless, μeV tunnel couplings seem possible. An entangling gate will take only a few nanoseconds but requires subnanosecond pulses.

The setup provides a rich variety of leakage states. Appendix B introduces an extended state basis in $s_z = 1$. I consider the charge configurations (1,2,1,2), (1,2,2,1), and (1,1,2,2), while I neglect doubly occupied triplets at QD_1 and QD_3 (see Sec. II). The tunnel couplings are only relevant around state degeneracies in the gate construction, which is justified for vanishing τ_i, $i = 1, \ldots, 4$, compared to Ω_L and Ω_R. In reality, τ_i are small compared to Ω_L and Ω_R, but they are not negligible. As a consequence, modifications from the anticrossings partially lift the neighboring state crossings (see the blue and purple circles in Fig. 2) and modify the energy levels and anticrossings. Figure 3 shows that high-fidelity gates can be constructed that only have small leakage, when the

TABLE I. Summary of the state evolution that generates the CPHASE gate, as described in the text [cf. Eq. (4)]. All phase evolutions that can be corrected with single-qubit gates are neglected. (1) The states $|1_R\rangle$ and $|B\rangle$ interchange. (2) The transfer through a DLZC mixes the state $|1_L0_R\rangle$ to the subspace $\{|1_L0_R\rangle,|L\rangle,|E\rangle\}$. (3) The central part of the entangling operation introduces a nontrivial phase factor to $|0_L0_R\rangle$. (4) The content in $\{|1_L0_R\rangle,|L\rangle,|E\rangle\}$ is brought back to $|1_L0_R\rangle$ using the appropriate pulse shape. (5) $|B\rangle$ and $|1_R\rangle$ interchange.

$\|1_L1_R\rangle$		$\|1_LB\rangle$		$\|1_LB\rangle$		$\|1_LB\rangle$		$\|1_LB\rangle$		$\|1_L1_R\rangle$
$\|1_L0_R\rangle$	$\xrightarrow{(1)}$	$\|1_L0_R\rangle$	$\xrightarrow{(2)}$	$\{\|1_L0_R\rangle,\|L\rangle,\|E\rangle\}$	$\xrightarrow{(3)}$	$\{\|1_L0_R\rangle,\|L\rangle,\|E\rangle\}$	$\xrightarrow{(4)}$	$\|1_L0_R\rangle$	$\xrightarrow{(5)}$	$\|1_L0_R\rangle$
$\|0_L1_R\rangle$		$\|0_LB\rangle$		$\|0_LB\rangle$		$\|0_LB\rangle$		$\|0_LB\rangle$		$\|0_L1_R\rangle$
$\|0_L0_R\rangle$		$\|0_L0_R\rangle$		$\|0_L0_R\rangle$		$-\|0_L0_R\rangle$		$-\|0_L0_R\rangle$		$-\|0_L0_R\rangle$

waiting times and the waiting positions introduced earlier are adjusted numerically. Small leakage errors and minor deviations from a CPHASE gate are reached for $\tau_i/\Omega_{L,R} < 5\%$, $i = 1,\ldots,4$. I use $\Omega/h = \Omega_L/h = \Omega_R/h = 15$ GHz and $\tau/h = \tau_i/h = 0.5$ GHz, $i = 1,\ldots,4$ in the following noise analysis (see Ref. [19] for a similar noise discussion).

A. Charge noise

Charge traps of the heterostructure introduce low-frequency electric field fluctuations [21,22]. Their influence is weak for spin qubits, but it increases for charge qubits [23,24]. Consequently, HQs are protected from charge noise only in the idle configuration. Charge noise is modeled by a low-frequency energy fluctuation between different charge configurations. I introduce no fluctuations during one gate simulation, but use modifications between successive runs. The fluctuations follow a Gaussian probability distribution of rms $\delta\epsilon$. Note that the numerically optimized gate sequence of Eq. (4) is simulated.

Figure 4 shows the gate fidelity F, which is defined in Appendix A, while $\delta\epsilon$ is varied. F decreases rapidly with $\delta\epsilon$. A Gaussian decay is seen for small $\delta\epsilon$. The decay constant shows that τ is the relevant energy scale of the entangling gate. The coherence is lost if $\delta\epsilon$ increases beyond τ because a typical gate misses the anticrossings of Fig. 2. Noisy gate sequences keep only the diagonal entries of the density matrix, but they remove all off-diagonal entries leading to $F = 0.25$.

Charge noise can be modeled for QD spin qubits to cause energy fluctuations of $\delta\epsilon \approx \mu$eV ($1\ \mu\text{eV}/h \approx 0.2$ GHz). Both for GaA charge qubits [21] and Si charge qubits [25], current experiments suggest charge noise on the order of a few μeV. For high-fidelity pulse-gated entangling operations, $\delta\epsilon$ must be smaller than τ that reaches typically a few μeV in Si HQs.

B. Hyperfine interactions

Nuclear spins couple to HQs, and they cause low-frequency magnetic field fluctuations [26,27]. The error analysis can be restricted to the total $s_z = 1$ subspace when the global magnetic fields E_z are larger than the uncertainties in the magnetic field δE_z at every QD. Already global magnetic fields of 100 mT are much larger than the typical δE_z for Si QDs ($E_z/h > 3$ GHz (>100 mT) and $\delta E_z/h < 3$ MHz ($<100\ \mu$T) for Si QDs [28,29]). I simulate the numerically optimized pulse sequence of Eq. (4) under magnetic field fluctuations. The variations of the magnetic fields at every QD are determined

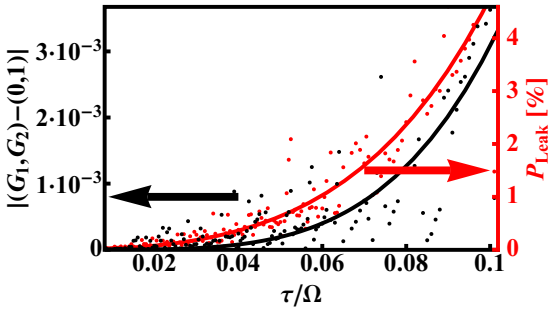

FIG. 3. (Color online) Numerically optimized gate sequences according to Eq. (4) for $\Omega = \Omega_L = \Omega_R$ and $\tau = \tau_i$, $i = 1,\ldots,4$. The deviations of the Makhlin invariants [20] from $G_1 = 0$ and $G_2 = 1$ and the leakage errors P_{Leak} are numerically minimized by adjusting the waiting times and waiting positions. $P_{\text{Leak}} = |U_{\mathcal{PQ}}|^2$ is the transition probability from the computational subspace $\mathcal{P}$ to the leakage subspace $\mathcal{Q}$. The points describe single numerical results; the solid lines are a polynomial fit. Note that small τ/Ω permit better gates.

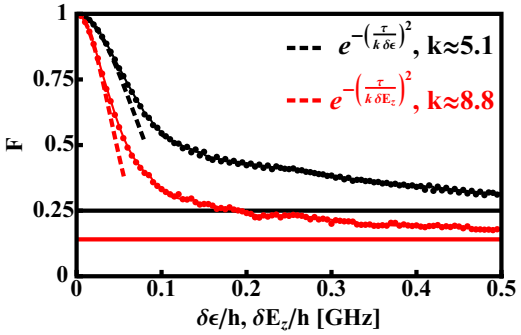

FIG. 4. (Color online) Fidelity analysis for the numerically optimized CPHASE gates under charge noise (black) and nuclear spin noise (red) at $\Omega_L/h = \Omega_R/h = 15$ GHz and $\tau/h = \tau_i/h = 0.5$ GHz, $i = 1,\ldots,4$. The energy fluctuations $\delta\epsilon$ between different charge configurations model charge noise. Nuclear spins cause local, low-frequency magnetic field fluctuations of the energy δE_z. Both noise sources can be described by a classical probability distribution with the rms $\delta\epsilon$ (for charge noise) and δE_z (for nuclear spin noise). The fidelity F is extracted from 1000 gate simulations according to Eq. (4). Increasing the uncertainties suppresses F strongly till it saturates at 0.25 (for charge noise) and 9/64 (for nuclear spin noise) (see the horizontal lines). The initial decay of F is described by a Gaussian decay law (see the dotted lines).

by a Gaussian probability distribution with the rms δE_z (in energy units).

Figure 4 shows that F decreases rapidly with δE_z. Again, a Gaussian decay is observed with a decay constant determined by τ for small δE_z. The influence of hyperfine interactions differs from charge noise. Local magnetic fields lift the state crossings that are protected by the spin-selection rules (see blue markings in Fig. 2). Not only is the coherence lost for large δE_z, but leakage further suppresses F. The limit of large δE_z can be approximated with $F = 9/64$. All off-diagonal entries of the density matrix are removed. Additionally, some states are mixed with leakage states. $|1_L 1_R\rangle$ goes to a mixed state with three other states; $|1_L 0_R\rangle$ and $|0_L 1_R\rangle$ mix with one other state each.

Si is a popular QD material because the number of finite-spin nuclei is small [15]. Nevertheless, noise from nuclear spins was identified to be dominant in the first spin qubit manipulations of gate-defined Si QDs [18]. $\delta E_z/h = 7.5 \times 10^{-4}$ GHz in natural Si (see Ref. [28]) is sufficient for nearly perfect two-qubit pulse gates. The fluctuations of the nuclear spins decrease further for isotopically purified Si instead of natural Si, a system which has shown rapid experimental progress recently [30,31]. We note that $\delta E_z/h = 30$ MHz for GaAs QDs would be problematic for high-fidelity entangling operations.

V. CONCLUSION

I have constructed a two-qubit pulse gate for the HQ—a qubit encoded in a three-electron configuration on a gate-defined DQD. Applying fast voltage pulses at gates close to the QDs enables the transfer of single electrons between QDs. The setup is tuned to the anticrossing of $|0_L 0_R\rangle$ with the leakage state $|E\rangle$. $|0_L 0_R\rangle$ picks up a nontrivial phase without leaking to $|E\rangle$, while all the other two-qubit states accumulate trivial phases. The main challenge of the entangling gate is to avoid leakage to other states. One can use a two-step procedure. (1) The right HQ is pulsed to the readout configuration. Here, $|1_R\rangle$ goes to (2,1), but $|0_R\rangle$ stays in (1,2). (2) $|0_L 1_R\rangle$ passes through a DLZC during the pulse cycle. The pulse profile is adjusted to avoid leakage after the full pulse cycle. Note that an adiabatic manipulation protocol can substitute the pulse-gated manipulation [32].

Cross-couplings between anticrossings, charge noise, and nuclear spin noise introduce errors for the pulse-gated two-qubit operation. Cross-couplings between anticrossings are problematic as they open state crossings. Also these mechanism slightly influence the energy levels and the sizes of the anticrossings. Reasonably small values of $\tau/\Omega \lesssim 5\%$ still permit excellent gates through pulse shaping. Charge noise is problematic because the gate tunes the HQs between different charge configurations. Current QD experiments suggest that charge noise is critical for the pulse-gated entangling operation. Nuclear spins are unimportant for the pulse-gated entangling operation of HQs in natural Si and, even more, for isotopically purified Si. I am hopeful that material improvements and advances in fabrication techniques for Si QDs still allow an experimental realization of this gate in the near future.

Pulse gates provide universal control of HQs through single-qubit operations, which have been implemented experimentally [3,4], together with the described two-qubit entangling gate. Because this setup can be scaled up trivially (see Fig. 1), further experimental progress should be stimulated to realize all-pulse-gated manipulations of HQs.

ACKNOWLEDGMENT

I thank D. P. DiVincenzo and L. R. Schreiber for many useful discussions.

APPENDIX A: FIDELITY DESCRIPTION OF NOISY GATES

U_n^ξ describes a noisy operation with a parameter ξ which modifies the gate between different runs of the experiment and obeys a classical probability distribution $f(\xi)$. The entanglement fidelity is a measure for the gate performance [33,34]:

$$F(\xi) = \mathrm{tr}\left\{\rho^{RS}\mathbf{1}_R \otimes \left[U_i^{-1}U_n^\xi\right]_S \rho^{RS}\mathbf{1}_R \otimes \left[\left(U_n^\xi\right)^{-1}U_i\right]_S\right\}. \tag{A1}$$

U_i describes the ideal time evolution. The state space is doubled to two identical Hilbert spaces R and S. $\rho^{RS} = |\psi\rangle\langle\psi|$ is a maximally entangled state on the larger Hilbert space; e.g., $|\psi\rangle = (|0000\rangle + |0110\rangle + |1001\rangle + |1111\rangle)/2$. The gate fidelity F is calculated by averaging Eq. (A1) over many instances of U_n^ξ, giving $F = \int d\xi f(\xi)F(\xi)$. $F = 1$ for perfect gates. This definition captures also leakage errors.

APPENDIX B: EXTENDED BASIS

Table II provides an extended state basis in $s_z = 1$ for the description of two HQs in (1,2,1,2), (1,2,2,1), and (1,1,2,2). States with a doubly occupied triplet at QD_1 or QD_3 are neglected because the triplet configurations at QD_1 and QD_3 are assumed to require much higher energies than the singlet configurations (see Sec. II). $|1_L 1_R\rangle$, $|1_L 0_R\rangle$, $|0_L 1_R\rangle$, and $|0_L 0_R\rangle$ are the computational basis of two HQs. The states $|L\rangle$, $|1_L B\rangle$, and $|0_L B\rangle$ are partially filled during the manipulation procedure. All other states are leakage states that are ideally unfilled during the manipulation. The states describe the spin configurations at QD_i, $i = 1,\ldots,4$, of the array of four QDs, and they are grouped into subspaces of equal energies.

It is straightforward to prove that the 23 states in Table II are a complete set to describe the six-electron spin problem of two HQs. Note that the discussion is restricted to total $s_z = 1$. One needs two additional spin-↑ electrons compared to the spin-↓ electrons in the (1,2,1,2) configuration, giving in total $\binom{6}{4} = 15$ choices. In the (1,2,2,1) and (1,1,2,2) configurations, the electrons at QD_2 and at QD_4 are always paired to a singlet state (because it is strongly unfavored to reach a triplet at these QDs), giving $\binom{4}{3} = 4$ choices to reach in total $s_z = 1$.

TABLE II. Extended state basis with the total spin quantum number $s_z = 1$ for the setup of six electrons distributed over four QDs. Each entry of the states describes a spin configuration at one of the QDs with the notation $|\mathrm{QD}_1,\mathrm{QD}_2,\mathrm{QD}_3,\mathrm{QD}_4\rangle$. All the relevant states for the electron configurations $(n_{\mathrm{QD}_1},n_{\mathrm{QD}_2},n_{\mathrm{QD}_3},n_{\mathrm{QD}_4}) = (1,2,1,2)$, $(1,2,2,1)$, and $(1,1,2,2)$ are included. Further details are given in the text.

	state	energy
(1,2,1,2)	$\lvert 1_L 1_R\rangle = \left[\sqrt{\frac{2}{3}}\lvert\downarrow T_+\rangle - \sqrt{\frac{1}{3}}\lvert\uparrow T_0\rangle\right]\left[\sqrt{\frac{2}{3}}\lvert\downarrow T_+\rangle - \sqrt{\frac{1}{3}}\lvert\uparrow T_0\rangle\right]$	$\Omega_L + \Omega_R$
	$\lvert\alpha_1\rangle = \left[\sqrt{\frac{1}{3}}\lvert\downarrow T_+\rangle + \sqrt{\frac{2}{3}}\lvert\uparrow T_0\rangle\right]\left[\sqrt{\frac{2}{3}}\lvert\downarrow T_+\rangle - \sqrt{\frac{1}{3}}\lvert\uparrow T_0\rangle\right]$	
	$\lvert\alpha_2\rangle = \left[\sqrt{\frac{2}{3}}\lvert\downarrow T_+\rangle - \sqrt{\frac{1}{3}}\lvert\uparrow T_0\rangle\right]\left[\sqrt{\frac{1}{3}}\lvert\downarrow T_+\rangle + \sqrt{\frac{2}{3}}\lvert\uparrow T_0\rangle\right]$	
	$\lvert\alpha_3\rangle = \left[\sqrt{\frac{1}{3}}\lvert\downarrow T_+\rangle + \sqrt{\frac{2}{3}}\lvert\uparrow T_0\rangle\right]\left[\sqrt{\frac{1}{3}}\lvert\downarrow T_+\rangle + \sqrt{\frac{2}{3}}\lvert\uparrow T_0\rangle\right]$	
	$\lvert\alpha_4\rangle = \lvert\uparrow T_- \uparrow T_+\rangle$	
	$\lvert\alpha_5\rangle = \lvert\uparrow T_+ \uparrow T_-\rangle$	
	$\lvert\alpha_6\rangle = \lvert\uparrow T_+ \downarrow T_0\rangle$	
	$\lvert\alpha_7\rangle = \lvert\downarrow T_0 \uparrow T_+\rangle$	
	$\lvert 1_L 0_R\rangle = \left[\sqrt{\frac{2}{3}}\lvert\downarrow T_+\rangle - \sqrt{\frac{1}{3}}\lvert\uparrow T_0\rangle\right]\lvert\uparrow S\rangle$	Ω_L
	$\lvert L\rangle = \left[\sqrt{\frac{1}{6}}\lvert\uparrow T_0 \uparrow\rangle - \frac{\sqrt{3}}{2}\lvert\uparrow T_+ \downarrow\rangle + \frac{1}{2\sqrt{3}}\lvert\downarrow T_+ \uparrow\rangle\right]\lvert S\rangle$	
	$\lvert\beta\rangle = \left[\frac{1}{2}\lvert\uparrow T_+ \downarrow\rangle + \frac{1}{2}\lvert\downarrow T_+ \uparrow\rangle + \sqrt{\frac{1}{2}}\lvert\uparrow T_0 \uparrow\rangle\right]\lvert S\rangle$	
	$\lvert 0_L 1_R\rangle = \lvert\uparrow S\rangle\left[\sqrt{\frac{2}{3}}\lvert\downarrow T_+\rangle - \sqrt{\frac{1}{3}}\lvert\uparrow T_0\rangle\right]$	Ω_R
	$\lvert\gamma_1\rangle = \lvert\uparrow S\rangle\left[\sqrt{\frac{1}{3}}\lvert\downarrow T_+\rangle + \sqrt{\frac{2}{3}}\lvert\uparrow T_0\rangle\right]$	
	$\lvert\gamma_2\rangle = \lvert\downarrow S \uparrow T_+\rangle$	
	$\lvert 0_L 0_R\rangle = \lvert\uparrow S \uparrow S\rangle$	0
(1,2,2,1)	$\lvert 1_L B\rangle = \left[\sqrt{\frac{2}{3}}\lvert\downarrow T_+\rangle - \sqrt{\frac{1}{3}}\lvert\uparrow T_0\rangle\right]\lvert S \uparrow\rangle$	$\Delta_{43} + \Omega_L$
	$\lvert\delta_1\rangle = \left[\sqrt{\frac{1}{3}}\lvert\downarrow T_+\rangle + \sqrt{\frac{2}{3}}\lvert\uparrow T_0\rangle\right]\lvert S \uparrow\rangle$	
	$\lvert\delta_2\rangle = \lvert\uparrow T_+ S \downarrow\rangle$	
	$\lvert 0_L B\rangle = \lvert\uparrow SS \uparrow\rangle$	Δ_{43}
(1,1,2,2)	$\lvert\mu_1\rangle = \lvert\uparrow\uparrow ST_0\rangle$	$\Delta_{23} + \Omega_R$
	$\lvert\mu_2\rangle = \lvert\uparrow\downarrow ST_+\rangle$	
	$\lvert\mu_3\rangle = \lvert\downarrow\uparrow ST_+\rangle$	
	$\lvert E\rangle = \lvert\uparrow\uparrow SS\rangle$	Δ_{23}

[1] Z. Shi, C. B. Simmons, J. R. Prance, J. K. Gamble, T. S. Koh, Y.-P. Shim, X. Hu, D. E. Savage, M. G. Lagally, M. A. Eriksson, M. Friesen, and S. N. Coppersmith, Phys. Rev. Lett. **108**, 140503 (2012).

[2] T. S. Koh, J. K. Gamble, M. Friesen, M. A. Eriksson, and S. N. Coppersmith, Phys. Rev. Lett. **109**, 250503 (2012).

[3] Z. Shi, C. B. Simmons, D. R. Ward, J. R. Prance, X. Wu, T. S. Koh, J. K. Gamble, D. E. Savage, M. G. Lagally, M. Friesen,

S. N. Coppersmith, and M. A. Eriksson, Nat. Commun. **5**, 3020 (2014).

[4] D. Kim, Z. Shi, C. B. Simmons, D. R. Ward, J. R. Prance, T. S. Koh, J. K. Gamble, D. E. Savage, M. G. Lagally, M. Friesen, S. N. Coppersmith, and M. A. Eriksson, Nature (London) **511**, 70 (2014).

[5] D. P. DiVincenzo, D. Bacon, J. Kempe, G. Burkard, and K. B. Whaley, Nature (London) **408**, 339 (2000).

[6] B. H. Fong and S. M. Wandzura, Quantum Inf. Comput. **11**, 1003 (2011).

[7] R. Hanson and G. Burkard, Phys. Rev. Lett. **98**, 050502 (2007).

[8] M. D. Shulman, O. E. Dial, S. P. Harvey, H. Bluhm, V. Umansky, and A. Yacoby, Science **336**, 202 (2012).

[9] F. W. Strauch, P. R. Johnson, A. J. Dragt, C. J. Lobb, J. R. Anderson, and F. C. Wellstood, Phys. Rev. Lett. **91**, 167005 (2003).

[10] L. DiCarlo, J. M. Chow, J. M. Gambetta, L. S. Bishop, B. R. Johnson, D. I. Schuster, J. Majer, A. Blais, L. Frunzio, S. M. Girvin, and R. J. Schoelkopf, Nature (London) **460**, 240 (2009).

[11] L. DiCarlo, M. D. Reed, L. Sun, B. R. Johnson, J. M. Chow, J. M. Gambetta, L. Frunzio, S. M. Girvin, M. H. Devoret, and R. J. Schoelkopf, Nature (London) **467**, 574 (2010).

[12] R. Barends, J. Kelly, A. Megrant, A. Veitia, D. Sank, E. Jeffrey, T. C. White, J. Mutus, A. G. Fowler, B. Campbell, Y. Chen, Z. Chen, B. Chiaro, A. Dunsworth, C. Neill, P. O'Malley, P. Roushan, A. Vainsencher, J. Wenner, A. N. Korotkov, A. N. Cleland, and J. M. Martinis, Nature (London) **508**, 500 (2014).

[13] T. Usuki, Phys. Rev. B **56**, 13360 (1997).

[14] G. S. Vasilev, S. S. Ivanov, and N. V. Vitanov, Phys. Rev. A **75**, 013417 (2007).

[15] F. A. Zwanenburg, A. S. Dzurak, A. Morello, M. Y. Simmons, L. C. L. Hollenberg, G. Klimeck, S. Rogge, S. N. Coppersmith, and M. A. Eriksson, Rev. Mod. Phys. **85**, 961 (2013).

[16] Note that $|\bar{i}\rangle$ can be an orbital excited state or a valley excited state in Si. $|2\rangle$ and $|\bar{2}\rangle$ determine the energy difference between $|0_L\rangle$ and $|1_L\rangle$. The described two-qubit gate relies on a larger singlet-triplet energy difference for the two-electron configuration at QD_1 compared to QD_2. Equivalent discussions hold for HQ_R. In contrast, GaAs QDs lack valley excited states; one can realize the same entangling gate using one large QD and one small QD. Then, the energy difference between the two-electron singlet and the two-electron triplet depends on the confining strength of the wave functions.

[17] X. Wu, D. R. Ward, J. R. Prance, D. Kim, J. K. Gamble, R. T. Mohr, Z. Shi, D. E. Savage, M. G. Lagally, M. Friesen, S. N. Coppersmith, and M. A. Eriksson, Proc. Natl. Acad. Sci. USA **111**, 11938 (2014).

[18] B. M. Maune, M. G. Borselli, B. Huang, T. D. Ladd, P. W. Deelman, K. S. Holabird, A. A. Kiselev, I. Alvarado-Rodriguez, R. S. Ross, A. E. Schmitz, M. Sokolich, C. A. Watson, M. F. Gyure, and A. T. Hunter, Nature (London) **481**, 344 (2012).

[19] S. Mehl, H. Bluhm, and D. P. DiVincenzo, Phys. Rev. B **90**, 045404 (2014).

[20] Y. Makhlin, Quantum Inf. Process. **1**, 243 (2002).

[21] K. D. Petersson, J. R. Petta, H. Lu, and A. C. Gossard, Phys. Rev. Lett. **105**, 246804 (2010).

[22] O. E. Dial, M. D. Shulman, S. P. Harvey, H. Bluhm, V. Umansky, and A. Yacoby, Phys. Rev. Lett. **110**, 146804 (2013).

[23] X. Hu and S. Das Sarma, Phys. Rev. Lett. **96**, 100501 (2006).

[24] S. Mehl and D. P. DiVincenzo, Phys. Rev. B **88**, 161408 (2013).

[25] Z. Shi, C. B. Simmons, D. R. Ward, J. R. Prance, R. T. Mohr, T. S. Koh, J. K. Gamble, X. Wu, D. E. Savage, M. G. Lagally, M. Friesen, S. N. Coppersmith, and M. A. Eriksson, Phys. Rev. B **88**, 075416 (2013).

[26] J. M. Taylor, J. R. Petta, A. C. Johnson, A. Yacoby, C. M. Marcus, and M. D. Lukin, Phys. Rev. B **76**, 035315 (2007).

[27] R. Hanson, L. P. Kouwenhoven, J. R. Petta, S. Tarucha, and L. M. K. Vandersypen, Rev. Mod. Phys. **79**, 1217 (2007).

[28] L. V. C. Assali, H. M. Petrilli, R. B. Capaz, B. Koiller, X. Hu, and S. Das Sarma, Phys. Rev. B **83**, 165301 (2011).

[29] Also GaAs QDs would fulfill this condition with $E_z/h >$ 0.5 GHz (>100 mT) and $\delta E_z/h <$ 30 MHz (<5 mT), which describes an uncorrected nuclear spin bath.

[30] M. Veldhorst, J. C. C. Hwang, C. H. Yang, A. W. Leenstra, B. de Ronde, J. P. Dehollain, J. T. Muhonen, F. E. Hudson, K. M. Itoh, A. Morello, and A. S. Dzurak, Nat. Nanotechnol. **9**, 981 (2014).

[31] M. Veldhorst, C. H. Yang, J. C. C. Hwang, W. Huang, J. P. Dehollain, J. T. Muhonen, S. Simmons, A. Laucht, F. E. Hudson, K. M. Itoh, A. Morello, and A. S. Dzurak, arXiv:1411.5760.

[32] All energy levels follow the lowest energy states for adiabatic manipulation protocols. The nontrivial part of the entangling gate is also obtained at the degeneracy of $|0_L 0_R\rangle$ with $|E\rangle$. The pulse shape must compensate for the pulsing through the DLZC of $\{|1_L 0_R\rangle, |L\rangle, |E\rangle\}$.

[33] M. A. Nielsen and I. L. Chuang, *Quantum Computation and Quantum Information* (Cambridge University Press, Cambridge, 2000).

[34] D. C. Marinescu and G. M. Marinescu, *Classical and Quantum Information* (Elsevier, Amsterdam, 2012).